Article

Chinese Science Bulletin

Geochemistry

August 2010 Vol.55 No.24: 2684–2696
doi: 10.1007/s11434-010-3231-3

A peculiar composite M- and W-type REE tetrad effect: Evidence from the Shuiquangou alkaline syenite complex, Hebei Province, China

ZHAO ZhenHua*, BAO ZhiWei & QIAO YuLou

Key Laboratory for Metallogenic Dynamics, Guangzhou Institute of Geochemistry, Chinese Academy of Sciences, Guangzhou 510640, China

Received August 14, 2009; accepted January 14, 2010

A new type of REE tetrad effect, a composite M- and W-type, was recognized in the K-feldsparthized and silicificated Shuiquangou alkaline syenites, Dongping, Hebei Province. Different analytical methods such as ICP-MS and isotopic dilution thermal ion mass spectrometer were exploited to verify the REE concentrations of the samples in three laboratories in China, France and Korea. The results are reliable and consistent within errors. *In situ* quantitative analysis of REE concentrations of individual zircons and apatites extracted from the very same sample has shown that fractional crystallization of magma and the superimposed hydrothermal alteration might have taken place in at least two-stage hydrothermal activities to generate the composite M- and W-type REE tetrad effect. The coexisting melt and aqueous phases, the superimposed alteration by volatile (Cl, CO_2)$^-$ and Si, K, Al-enriched high temperature hydrothermal fluids might be the important facts for this new MW-type of REE tetrad effect. In addition, the peculiar MW-type tetrad effect might be an indicator for Au mineralization of reworked plutons.

REE tetrad effect, MW-type of REE tetrad effect, apatite, zircon, Shuiquangou alkaline syenite

Citation: Zhao Z H, Bao Z W, Qiao Y L, et al. A peculiar composite M- and W-type REE tetrad effect: Evidence from the Shuiquangou alkaline syenite complex, Hebei Province, China. Chinese Sci Bull, 2010, 55: 2684–2696, doi: 10.1007/s11434-010-3231-3

The plot of chondrite-normalized REE abundances *vs.* atomic numbers exhibiting smooth linear or curvilinear trend, which is known as Masuda-Coryell diagram [1–3] has been applied broadly in geochemical researches for decades. The slop of the pattern ($(La/Yb)_N$), the relative enrichment or depletion of Ce and Eu ($Ce/^*Ce$; $Eu/^*Eu$), and the REE partition coefficients have become the basic parameters of REE geochemistry. However, ever since 1979, tetrad effects have been recognized in seawater, algae, sponges shells, limestones, etc. [4], hydrothermal uranium mineral-uraninite [5], REE mineral-kimuraite [6] and groundwater from peculiar geological occurrences [7]. Zhao and Masuda [8–10] first recognized M-type REE tetrad effect in rare-metal granites from South China in 1988.

The REE tetrad effect means that the chondrite-normalized REE patterns show four convex or concave sectors (La-Ce-Pr-Nd, Pm-Sm-Eu-Gd, Gd-Tb-Dy-Ho, Er-Tm-Yb-Lu) separated at Nd/Pm, Gd and Ho/Er (Figure 1) due to physical and chemical properties of REE changes coherently with the changes of electronic configuration of the atoms, which were named M-and W-type, respectively [11].

Shifting from the normal linear trend of chondrite-normalized REE patterns, REE tetrad effect must be an indication of peculiar geochemical processes involved. The phenomenon was first discovered in an experiment of REE partitioning in a pure chemical liquid-liquid extraction system [12,13]. The rare-metal mineralized granites showing REE tetrad effect are commonly highly evolved leucogranites. Highly fractional crystallization lead to the enrichment of volatiles (F, H_2O, Cl) in residual melts which may result in a transition system consists of co-existing magmatic melt and hydrothermal fluid. The Fluid/melt interaction in the system results in the M-type tetrad effect [8–10,14,15]. Some accessory REE minerals such as mona-

*Corresponding author (email: zhzhao@gig.ac.cn)

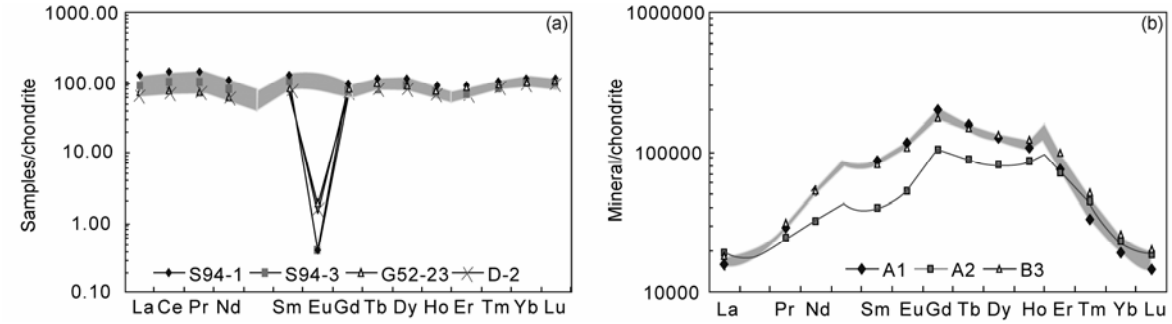

Figure 1 M-type REE tetrad effect in rare-metal granites [8–10] (a) and W-type REE tetrad effect in kimuraite [6] (b).

zite and xenotime were reported to show and/or control the REE tetrad effect [16–19]. Bau [19] argued that in principle the behavior of REEs should be controlled by their charge and radius (CHARRAC), for systems bearing lanthanide tetrad effect which show non-chondritic Y/Ho (>28) and Zr/Hf (<25) ratios there must have been some other special causes. These systems are commonly magmas of highly evolved and enriched in H_2O, Li, B, F, P and/or Cl. The REE tetrad effects in peraluminous granites of mid-eastern Germany suggest the increasing importance of an aqueous-like fluid system during the final stages of granite crystallization and REE fluorine complexation may play an important role. The complexation with fluorine is interpreted as major cause for Y/Ho>28, while the complexation with bicarbonate is assumed to generate Y/Ho values <28. Because REE accessory minerals commonly inherit the REE signature of the magma system, they are not the cause of REE tetrad effect [20].

Systematic investigations were carried out on the biotite granite from Qianlishan, Hunan Province and riebeckite granite from Baerzhe, Inner Mongolia, both of them display typical M-type REE tetrad effect [21,22]. Similar M-type REE tetrad effects were observed in whole-rock samples and their constituent minerals as well in the Qianlishan and Baerzhe granites. Consequently, the tetrad effect represents the integrated behavior of the whole system (including all the individual phase) of the rocks. It is evident that the tetrad effect becomes more obvious and pronounced with the increase in degree of magma fractionation.

The REE tetrad effect observed in the late Hercynian granite from the Erzgebirge Sn province, Germany may be inherited from an external fluid that might have influenced the system during and/or after the emplacement of the magma and it is unlikely that the convex tetrad effect in the samples can be explained by removal of a complementary REE pattern by a coexisting hydrothermal fluid [23].

Weak REE tetrad effect in the Altay No. 3 granite pegmatite in Xinjiang, China and it is weakly altered wall rock (amphibolite) as well reveals that the water/rock (fluid/melt) interaction would be favorable for producing the REE tetrad effect [24]. Clear convex tetrad effect of apatite and associated minerals, such as beryl, spodumene, tourmaline, alkali feldspar and spessartine in the pegmatite is observed, which represents intrinsic features of initial pegmatite magma and an external fluid bearing tetrad effect were produced during magma crystallization before fluid exsolution from the magma [25].

Minerals like stibnite and scheelite from low temperature strata-bound stibnite deposits and low-middle temperature strata-bound Au-Sb-W deposits in west Hunan Province, commonly show M-type of REE tetrad effect [25,26]. These deposits have no spatially or temporally relation with granites. The mineralization agent, fluorine, may be the cause for the tetrad effect [26]. Conjugate M- and W-type of tetrad effect were all observed in the uranium mineralized granites, sedimentary rocks and groundwater in the Tono area, central Japan, the granitic rocks show M-type tetrad effect while the groundwater and the sedimentary rocks exhibit W-type tetrad effect [7]. By contrast, some monazites from hydrothermal deposits possess W-type tetrad effect [27] while river sediments in north China show M-type tetrad effect that might have resulted from interactions between water and sedimentary grains during the weathering and transportation [28].

Experiments by Veksler et al. [29] demonstrated that REE partitioning between immiscible silicate melt and aluminoufluoride (cryolite Na_3AlF_6) melt may result in REE tetrad effect. Experiments on the structure and stability of aqueous rare-earth elements in hydrothermal fluids under condition up to 500 and 520 MPa reveal that the mobility and fractionation of REEs are controlled by the availability of and the degree of complexation with ligands such as Cl^-, F^-, PO_3^-, CO_3^- and SO_4^{2-}, the pH and redox conditions of the fluids [30]. The stability of complex ($Nd(H_2O)_{\delta-N}Cl_n^{+3-n}$) formed by Nd aqua ion with Cl is higher than theoretical prospect. The reduction of water molecules in the first coordination shell of the Nd^{+3} aqua ion is intermediate between the rate of Gd, Eu and Yb (Yb>Eu>Nd>Gd) indicating intermediate stability of Nd^{+3} aqua ion which is consistent with the tetrad effect [30].

In summary, our knowledge about REE tetrad effect can be concluded as follows: (1) the tetrad effects do exist in some peculiar rocks, water and sea shells, which are neither analytical artifacts nor crystallization of REE accessory minerals; (2) the REE tetrad effect can be found in the highly

evolved magmatic system and related mineralized granites, pegmatite, skarn, hydrothermally reworked strata-bound deposits and water system as well; (3) the tetrad effect can be divided into M- and W-type; and (4) highly evolved magmatic system, interactions between magma and volatile-rich (Cl,F,CO_2) fluids, and fluids (including hydrothermal fluid) may contribute to the generation of tetrad effect.

It is important to notice that the reported cases are M- or W-type tetrad effects occurring separately in natural systems, however, the composite M- and W-type REE tetrad effect reported in this paper is a brand new type of coexistence of M- and W-type tetrad effect in the very system. Thus, our study is surely an important step towards thorough understanding the REE tetrad effect [31].

1 Discovery of a peculiar composite M- and W-type REE tetrad effect

1.1 Composite M- and W-type REE tetrad effect

The author first recognized [31] that the peculiar chondrite-normalized REE patterns of K-feldsparthized and silicificated alkaline syenites in Shuiquangou, Dongping gold deposit, Hebei Province, which display nearly horizontal sine-form curves (Figure 2(b), (c)) that are obviously different from the smooth right declined (LREE enriched) patterns of the amphibole alkaline syenite in the same pluton (Figure 2(a); Table 1). What is more, the patterns are different from those of the M-type tetrad effect in rare-metal granites and the W-type tetrad effect in kimuraite (Figure 1). This peculiar REE pattern bears features of M- and W-type tetrad effects in the very same sample, in which the first four elements La-Ce-Pr-Nd show the firs subgroup of a typical M-type tetrad effect (1/2 M), the second four elements Pm-Sm-Eu-Gd show a transition of M- and W-type tetrad effects, indeed, some samples show obviously either the second subgroup of M-type tetrad effect or W-type tetrad effect (1/2M or 1/2W); the third group Gd-Tb-Dy-Ho and the fourth group Er-Tm-Yb-Lu exhibit the features of the third subgroup and the fourth subgroup of W-type tetrad effect (2/2 W). These features constitute a brand new type tetrad effect, i.e., the coexistence of M- and W-type tetrad effects in the very same sample (1/2M+transition+2/2W; 1/2M+3/2W; 2/2M+2/2W). Using the quantification methods of the tetrad effect performed by Irber [20] and Moneck et al. [23], we calculated the ratios of chondrite-normalized values of concentrations of the two central elements B,C, such as Ce and Pr; Tb and Dy (Ce_N, Pr_N, Tb_N, Dy_N) with the strait line interpolation values (Ce^*, Pr^*, Tb^*, Dy^*) of the first and the last elements in every subgroup of tetrad effects (Ce_N/Ce^*, Pr_N/Pr^*, Tb_N/Tb^*, Dy_N/Dy^*). The samples with ratios larger than 1 are considered to show M-type tetrad effect while samples with ratios less than 1 show W-type tetrad effect. The size of the tetrad effect (T_1, T_3 and t_1, t_3) were calculated using the methods suggested by Moneck and Irber, respectively (Table 2). Unsurprisingly, the parameters of central element of the first subgroup such as Ce_N/Ce^*, Pr_N/Pr^* are both high than unit which indicate M-type tetrad effect, and the parameters of central elements of the third subgroup Tb_N/Tb^*, Dy_N/Dy^* are obviously low than unit which signify W-type tetrad effect. Accordingly, T_1 and T_3 values ($T_1>1$, $0<T_3<1$; $t_1>1$, $t_3<1$) also signify M- type tetrad effect in the first subgroup, W-type tetrad effect in the third subgroup, and weak W-type tetrad effect in the fourth subgroup.

1.2 Analytical method

Different analytical methods such as ICP-MS and isotopic dilution thermal ion mass spectrometer (ID-TIMS)were carried out at three laboratories in China, France (CRPG, Nancy) and Korea (Environmental Geology Division, Kigan, Daejeon) to confirm the REE concentrations of these samples. Considering the possible influence of some accessory minerals on the tetrad effect, different dissolving reagents

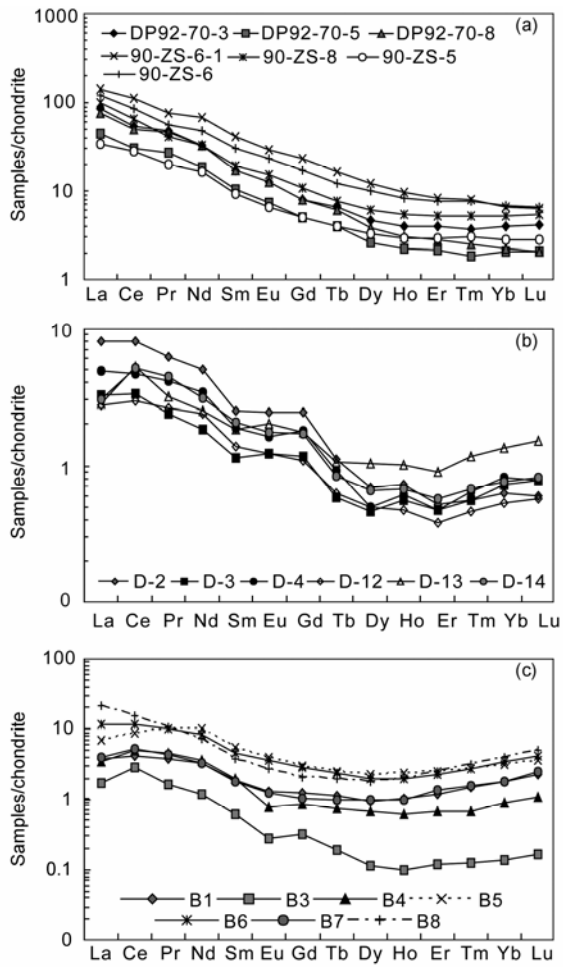

Figure 2 Comparison of the composite M- with W-type tetrad effect in K-feldsparthized and silicificatized alkaline syenites with the LREE enriched right declined patterns of amphibole alkaline syenites. (a) Shuiquangou amphybole alkaline syenites; (b) and (c) potassic-silicificated alkaline syenites.

Table 1 Major and REE concentrations of the Shuiquangou alkaline syenite (major element in %, REE in μg/g)[a)]

Sample No.	B1	B3	B4	B5	B6	B7	B8	D-2	D-3	D-4	D-12	D-13	D-14	90HG-4	90HG-2	BDP-4	90ZS-6-1	90ZS-8	90ZS-6	90ZS-5	Dp92-70-3	Dp92-70-5	Dp92-70-8
SiO_2	71.27	66.18	63.96	64.93	64.56	73.48	72.9	64.96	77.06	65.6	70.69	64.92	65.5	65.86	72.99	70.45	60.79	63.12	59.92	64.58			
TiO_2	0.07	0.08	0.08	0.08	0.07	0.05	0.07	0.07	0.04	0.06	0.06	0.06	0.07	0.01	0.01	<D	0.46	0.29	0.48	0.11			
Al_2O_3	15.33	17.42	19.06	17.84	18.7	14.2	14.1	19.13	12.48	19.02	15.34	18.83	19.68	18.48	12.98	16.69	18.41	18.51	18.95	19.18			
Fe_2O_3	0.85	0.71	1.07	1.25	1.38	1.09	1.25	0.63	0.34	0.48	0.93	0.99	0.67	0.39	0.67	0.79	2.14	1.86	2.22	1.13			
FeO	0.31	0.29	0.28	0.37	0.32	0.32	0.35	0.93	1.23	1.12	1.56	1.23	1.12	0.32	0.42		1.77	1.30	2.19	0.44			
MnO	0.02	0.01	0.04	0.05	0.04	0.02	0.03							0.1	0.05	<D	0.17	0.14	0.17	0.06			
MgO	0.53	0.59	0.41	0.42	0.37	0.39	0.34							0.08	0.01	<D	0.70	0.80	1.10	0.01			
CaO	0.7	0.35	1.13	1.17	1.36	0.59	0.94	1.12	0.87	0.21	0.36	0.89	1.12	2.00	0.30	0.15	3.07	3.50	4.40	0.30			
Na_2O	5.31	5.38	6.27	6.49	6.88	4.64	4.80	6.03	4.53	5.77	5.23	5.96	6.07	6.13	4.00	5.93	5.00	5.50	5.40	4.15			
K_2O	5.01	8.89	6.95	6.63	5.44	4.51	4.54	5.29	3.80	6.15	5.29	5.94	5.12	5.70	9.70	5.61	5.60	3.50	4.05	8.75			
H_2O+	0.30	0.41	0.20	0.23	0.37	0.20	0.22							0.29	0.55	0.63	0.41	0.77	0.26	0.78			
P_2O_5	0.02	0.01	0.02	0.02	0.03	0.03	0.02							0.01	0.001	0.05	0.09	0.12	0.20	0.01			
Total	99.52	100.3	99.47	99.48	99.52	99.52	99.56							99.37	101.68	100.5	99.24	99.41	99.34	99.5			
La	0.80	0.52	1.10	1.04	2.00	1.57	3.30	2.53	1.02	1.50	0.86	0.88	0.95	1.18	0.88	1.47	44.38	31.35	38.25	10.63	26.95	14.03	23.71
Ce	2.91	2.32	5.80	4.73	5.57	4.98	6.54	6.53	2.7	3.75	2.38	4.21	4.19	3.25	2.63	4.40	92.12	52.61	70.49	22.57	44.14	24.47	41.06
Pr	0.34	0.20	0.60	0.75	0.88	0.53	0.74	0.75	0.29	0.51	0.32	0.39	0.54	0.56	0.41	0.50	9.78	4.98	6.97	2.43	5.87	3.28	5.61
Nd	1.35	0.71	2.64	3.45	3.37	1.73	2.40	3.00	1.11	2.06	1.43	1.50	1.87	2.12	1.53	2.00	40.56	19.92	28.59	9.76	19.93	11.29	19.62
Sm	0.29	0.12	0.6	0.74	0.71	0.32	0.45	0.49	0.22	0.37	0.27	0.36	0.4	0.37	0.33	0.43	8.18	3.75	5.84	1.79	3.39	1.99	3.39
Eu	0.092	0.02	0.21	0.24	0.23	0.15	0.15	0.18	0.09	0.12	0.091	0.15	0.13	0.09	0.097	0.037	2.18	1.14	1.72	0.49	0.92	0.55	0.91
Gd	0.24	0.08	0.50	0.60	0.55	0.26	0.38	0.64	0.30	0.46	0.28	0.45	0.44	0.25	0.35	0.37	5.94	2.77	4.45	1.32	2.08	1.28	2.05
Tb	0.04	0.01	0.08	0.1	0.09	0.05	0.07	0.053	0.028	0.044	0.03	0.05	0.04	0.04	0.064	0.057	0.77	0.36	0.58	0.19	0.31	0.19	0.29
Dy	0.23	0.04	0.42	0.58	0.52	0.29	0.43	0.22	0.15	0.16	0.16	0.33	0.21	0.21	0.42	0.32	3.85	1.98	3.19	1.06	1.47	0.84	1.22
Ho	0.056	0.007	0.091	0.14	0.12	0.071	0.11	0.052	0.04	0.044	0.034	0.072	0.049	0.045	0.091	0.07	0.7	0.39	0.6	0.21	0.29	0.16	0.22
Er	0.2	0.03	0.3	0.47	0.42	0.25	0.42	0.11	0.1	0.1	0.08	0.19	0.12	0.15	0.28	0.21	1.74	1.08	1.6	0.61	0.84	0.46	0.59
Tm	0.04	0.01	0.05	0.08	0.08	0.05	0.09	0.018	0.018	0.021	0.015	0.038	0.022	0.03	0.043	0.039	0.26	0.17	0.24	0.1	0.12	0.064	0.075
Yb	0.32	0.028	0.35	0.62	0.63	0.4	0.76	0.13	0.15	0.17	0.11	0.28	0.16	0.21	0.27	0.29	1.39	1.09	1.45	0.59	0.82	0.44	0.46
Lu	0.06	0.01	0.06	0.11	0.12	0.08	0.16	0.02	0.026	0.026	0.019	0.05	0.027	0.039	0.044	0.055	0.21	0.18	0.22	0.092	0.14	0.074	0.072
Y	1.82	0.19	3.02	4.62	4.13	2.39	4.05	1.33	0.99	1.27	0.74	1.71	1.12	1.62	2.91	2.31	17.48	10.59	15.63	5.29	8.51	4.17	6.50
∑REE	6.98	4.09	12.79	13.65	15.28	10.69	15.99	14.72	6.22	9.31	6.08	8.95	9.15	10.17	10.34	10.25	229.53	132.38	179.82	57.12	107.26	59.12	99.27
Eu/Eu*	1.08	0.63	1.16	1.11	1.10	1.12	1.07	0.99	1.08	0.9	1.02	1.15	0.96	0.88	0.87	0.34	0.96	1.08	1.03	0.98	1.06	1.05	1.06
$(La/Yb)_N$	1.68	12.44	2.11	1.12	2.14	2.63	2.92	13.0	5.3	6.7	5.2	2.1	4.0	3.79	2.18	3.40	21.53	19.39	17.85	12.11	22.10	21.69	34.98
Y/Ho	32.5	27.1	33.2	33.0	34.4	33.7	36.8	25.6	24.8	28.9	21.8	23.8	22.9	36.0	32.0	33.0	25.0	27.2	26.1	25.2	29.3	26.1	29.5

a) B_1–BDP-4, Potassic silicicated alkaline syenite; 90ZS-6-1–Dp92-70-8, alkaline syenite.

Table 2 Parameters of MW-type tetrad effect for Shuiquangou altered alkaline syenite[a)]

Sample No.	Ce_N/Ce^*	Pr_N/Pr^*	Tb_N/Tb^*	Dy_N/Dy^*	Tm_N/Tm^*	Yb_N/Yb^*	T_1	T_3	t_1	t_3
B1[9]	1.17	1.08	0.84	0.91	0.99	0.98	0.16	0.13	1.12	0.87
B3	1.93	1.23	0.86	0.73	0.92	0.80	0.68	0.68	1.52	0.79
B4	1.43	1.25	0.97	1.14	0.86	0.99	0.25	0.067	1.34	1.05
B5	1.15	1.18	0.92	0.88	0.96	0.99	0.17	0.10	1.16	0.90
B6	1.12	1.09	0.85	0.75	0.98	1.02	0.11	0.21	1.10	0.80
B7[151]	1.42	1.26	0.93	0.97	0.94	0.91	0.35	0.05	1.34	0.95
B8[57]	1.04	1.01	0.98	0.91	0.98	1.00	0.063	0.32	1.02	0.94
D2	1.17	1.04	0.68	0.62	1.02	1.08	0.12	0.35	1.10	0.65
D3	1.00	1.06	0.65	0.66	0.69	0.46	0.04	0.34	1.03	0.65
D4	1.08	1.09	0.74	0.57	1.32	1.09	0.08	0.35	1.08	0.79
D12	1.12	1.05	0.77	0.81	1.07	1.06	0.09	0.21	1.08	0.75
D13	1.91	1.45	0.67	0.85	1.09	1.06	0.66	0.26	1.66	
D14[173]	1.69	1.43	0.85	0.71	1.06	1.07	0.57	0.23	1.55	0.78
D15	1.61	1.05	0.67	0.80	1.19	1.13	0.45	0.27	1.69	0.73
BDP4	1.29	1.09	0.95	0.90	1.01	0.93	0.22	0.10	1.19	0.92

a) $Ce^*=La_N^{2/3}\times Nd_N^{1/3}$; $Pr^*=La_N^{1/3}\times Nd_N^{2/3}$; $Tb^{**}=Gb_N^{2/3}\times Ho_N^{1/3}$; $Dy^*=Gb_N^{1/3}\times Ho_N^{2/3}$; $T_1=\sqrt{1/2([Ce_N/Ce^*-1]^2+[Pr_N/Pr^*-1]^2)}$;

$T_2=\sqrt{1/2([Tb_N/Tb^*-1]^2+[Dy_N/Dy^*-1]^2)}$ (after Moneck et al. [23]) $t_1=[(Ce_N/Ce^*\times Pr_N/Pr^*)]^{0.5}$; $t_3=[(Tb_N/Tb^*\times Dy_N/Dy^*)]^{0.5}$ (after Irber [20]).

such as HF+HNO_3 and $Li_2B_2O_7$+H_3BO_3 were used in the analytical processes [32]. The results obtained via different methods of different laboratories are rather consistent within errors (Table 3), which confirm unanimously the existence of composite M- with W-type tetrad effect in the altered syenites (Figure 3).

2 Discussion on the generation of MW-type tetrad effect

LA-ICPMS *in situ* quantitative analysis of REE concentrations for individual zircons and apatites collected from the same K-feldsparthized and silicificated syenite (No.70 Au-bearing veins, 1200 m above sea level) were carried out (Tables 4 and 5). The analytical and data treatment methods follow the procedures reported by Yuan et al. [33]. Apatite is commonly present in igneous rocks as an main accessory mineral and a major REE carrier because of their high contents in whole rock (0.*n*%) and high apatite/melt REE partition coefficients (*n*–*n*×10). Generally speaking, there are no obvious preferential partition of REE into apatite lattice for various systems such as the apatite/aqueous fluid and apatite/silicate melt. Thus, the apatite is considered as entire REE partitioning mineral without obvious preferential cooperation of REEs except the slightly higher partition coefficient for the middle REEs Sm-Ho [34–38]. As a result, the apatite crystallization would not change dramatically the REE patterns of the melts or fluids, and consequently, the apatite can be considered as a potential indicator for magma or hydrothermal evolution. Zircon is very stable accessory mineral which may preserve its REE composition under magma conditions, however, hydrothermal alteration may significantly change the REE compositions of the zircons. It is reasonable to assume that the studies on the REE compositions of apatites and zircons collected from the K-feldsparthized and silicificated samples will contribute to our understanding of the generation of MW-type tetrad effect.

2.1 REE compositions of the apatites

The high contents of REE in the apatites are attributed to the substituting of Ca^{+2} with REE ($2REE^{+3} \rightarrow 3Ca^{+2}$) in apatite lattice ($Ca_3(PO_4)_3$(OH, F, Cl) for their similar ionic radius. The RE_2O_3 contents of apatite are usually 0.n%, the highest contents are found in apatites from alkaline pegmatite and syenite. The belovite $(Sr,Ce,Na,Ca)_3$ $(PO_4)_3(OH)$ is an extreme of apatite bearing REE content up12%.

LA-ICPMS *in situ* quantitative analysis of REE concentrations in individual apatite from the altered syenite bearing MW-type tetrad effect are listed in Table 4 and their important features are summarized as follows:

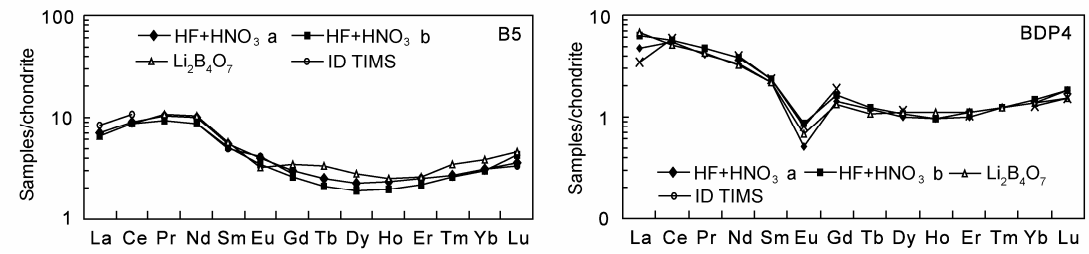

Figure 3 Comparison of REE patterns of the Shuiquangou alkaline syenites given by different analytical methods.

Table 3 Comparison of different analysis methods for the REE contents (μg/g) in Shuiquangou altered alkaline syenite

Sample No.	Potassic silicificated alkaline syenite B-5				Potassic silicificated alkaline syenite BDP-4			
Method	HF+HNO_3	HF+HNO_3 (France)	ID-TIMS(Korea)	$Li_2B_2O_7$+ H_2BO_3	HF+HNO_3	HF+HNO_3 (France)	ID-TIMS(Korea)	$Li_2B_2O_7$+ H_2BO_3
La	2.14	2.05	2.57	2.02	1.47	1.94	1.08	2.11
Ce	7.27	6.95	8.61	7.11	4.4	4.64	4.67	4.18
Pr	1.26	1.14		1.32	0.50	0.58		0.53
Nd	5.95	5.19	5.29	6.30	2.00	2.32	2.36	1.96
Sm	1.06	0.98	0.96	1.1	0.43	0.46	0.46	0.42
Eu	0.29	0.25	0.30	0.24	0.037	0.063	0.16	0.05
Gd	0.77	0.67	0.73	0.91	0.37	0.43	0.49	0.35
Tb	0.12	0.10		0.16	0.057	0.058		0.05
Dy	0.72	0.60	0.65	0.89	0.32	0.34	0.37	0.36
Ho	0.17	0.14		0.18	0.07	0.07		0.08
Er	0.52	0.46	0.47	0.55	0.21	0.23	0.22	0.23
Tm	0.088	0.085		0.11	0.04	0.04		0.04
Yb	0.66	0.63	0.64	0.80	0.29	0.31	0.27	0.29
Lu	0.12	0.14	0.11	0.15	0.06	0.06	0.05	0.05

The REE contents of the apatites are high ($\sum$REE+Y 1370–7100 μg/g) and can be divided into two groups: the first group is obviously LREE enriched and characterized by high $(La/Yb)_N$ ratios (70.5–256), high contents of $\sum$REE+Y (2495–7100 μg/g), without Eu anomalies (Eu/Eu^* 0.98–1.23), which is similar to that of unaltered alkaline syenite ($(La/Yb)_N$ 16.2–35.0; Eu/Eu^* 1.01–1.07) and shows the features of magmatic apatites (Figure 4(a), (b)). The second group is clearly enriched in the middle REE (Sm-Ho) and obviously depleted the LREE with $(Sm/La)_N$ 1.7–10.88, $(Gd/Yb)_N$ 7.20–8.13 and low contents of $\sum$REE+Y (1370–1674 μg/g), which display convex upward REE patterns that reflect a hydrothermal origin of the apatites (Figure 4(c)). The second group can again be divided into two subgroups, the first subgroup depleted evidently in LREE forming a typical W-type tetrad effect with $La_N<Ce_N<Pr_N<Nd_N<Sm_N<Eu_N > Gd_N$; the second subgroup is depleted in LREE to a less degree than that of the first subgroup, and exhibits REE patterns of composite M- and W-type tetrad effect. It possesses $La_N>Ce_N<Pr_N<Nd_N$, $Ce_N/Ce^* <1$, $Pr_N/Pr^*<1$ forming W-type tetrad effect and $Sm_N<Eu_N>Gd_N$, $Eu/Eu^*>1$ forming M-type tetrad effect.

2.2 REE compositions of zircons

Zircon is a physically and chemically stable and ubiquitously mineral which may be formed in high temperature situation like upper mantle to low temperature occurrences like hydrothermal fluids in crust. Recently, many studies reported that zircon may be crystallized from or altered by hydrothermal fluids [39–44]. Hydrothermal or hydrothermal altered zircons are potentially important for investigating the nature and timing of fluid flow and fluids/rock interaction. Thus, trace element particularly the REE compositions of the hydrothermal and altered zircons can be important tracer for the petrogenesis and mineralization processes. The hydrothermal zircon is texturally (base scatter emission-BSE and cathodoluminescence image–CL) and compositionally distinct from magmatic zircon [45–47]. Semilunar- or allotromorphic form, not clear prism, spongy inner texture and weak (and dark?) cathodoluminescence image are observed in hydrothermal zircons. Pronounced positive Ce anomaly existent in magmatic zircons. The reason for Ce anomaly is that under oxidizing conditions Ce mainly presents in +4 valence state Ce^{+4}. In general, +4 cations are preferentially incorporated into the lattice of zircon because the same valance and the Ce^{+4} is closer in size (0.097 nm) to Zr^{+4} (0.084 nm) than the neighbouring La^{+3} (0.116 nm) and Pr^{+3} (0.113 nm). In contrast, unlike their magmatic counterparts [43,48], hydrothermal or hydrothermal-altered zircons are characterized by higher REE contents, particularly LREEs, low oxygen fugacity and diminishing Ce anomaly. The chondrite-normalized REE patterns of the hydrothermal zircons exhibit flatter LREE patterns [$(Sm/La)_N$ 1.5–4.4 vs 22–110 for magmatic zircons] and diminishing Ce anomalies (Ce/Ce^* 1.8–3.5 vs 32–49 for magmatic zircon)[42].

Zircons from altered alkaline syenite are irregular grains or aggregate and show sponge or patch textures without oscillation or zoning on the cathodoluminescence images (Figure 5). Only few grains kept the texture of magmatic zircon. The altered zircons are significant enriched in $\sum$REE (509.7–9933 μg/g except one grain with 112.6 μg/g) and show chondrite-normalized REE patterns quite different to the magmatic zircons (Table 5; Figure 6). Positive Ce

Table 4 REE contents of apatites from altered alkaline syenite (μg/g)

No. of analysis point	APR21Q34	APR21Q35	APR21Q36	APR21Q37	APR21Q38	APR21Q39	APR21Q40	APR21Q41
La^{139}	1675.03	1544.4	371.17	616.41	1954.15	122.28	20.36	1053.29
Ce^{140}	2948.36	2639.83	793.66	1082.35	3440.22	279.63	121.95	2050.07
Pr^{141}	292.64	264.25	96.32	115.18	321.61	45.64	30.56	212.57
Nd^{143}	977.15	923.05	406.88	411.53	1050.14	271.8	225.12	704.35
Sm^{147}	89.66	95.58	103.91	55.66	98.14	131.2	139.43	77.08
Eu^{151}	21.97	23.16	41.94	17.03	24.89	58.88	69.61	20.39
Gd^{157}	49.11	54.77	103.86	40.44	52.08	155.14	174.18	48.8
Tb^{159}	5.36	6.17	14.16	4.7	5.03	22.34	24.63	5.88
Dy^{163}	22.28	27.67	61.9	21.71	21.22	96.98	102.47	26.48
Ho^{165}	3.58	4.64	9.24	3.76	3.49	14.23	14.39	4.34
Er^{166}	8.1	9.86	18.78	8.63	7.57	28.65	28	9.02
Tm^{169}	1.03	1.2	2.25	1.04	0.9	3.3	3.25	0.99
Yb^{173}	6.73	7.08	12.94	5.91	5.15	17.47	17.54	5.89
Lu^{175}	0.95	0.92	1.6	0.75	0.75	1.96	1.96	0.75
Ti^{49}	<0.63	<0.74	8.48	0.79	1.67	<0.49	<0.83	<0.92
Y^{89}	116.61	151.63	266.94	110	115.04	425.19	396.99	132.41
Zr^{90}	3.16	2.54	0.351	0.83	2.84	0.126	<0.028	1.77
Th^{232}	28.58	162.45	50.48	9.39	75.72	3.33	0.073	37.9
U^{238}	15.18	32.67	7.17	3.24	19.54	1.04	0.0223	10.78

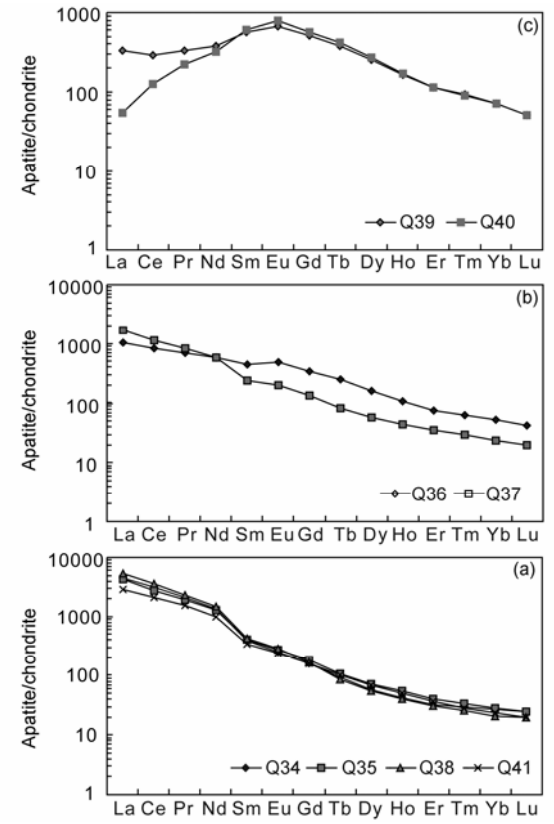

Figure 4 Chondrite-normalized REE patterns of apatites collected from K-feldsparthized and silicificated alkaline syenites.

anomaly similar to those of typical magmatic zircons exists only in three zircon grains (Ce/Ce^* 19.6–91.9) and diminishes to Ce/Ce^* 1.83–5.05 in the other grains. These Ce/Ce^* values are evidently lower than that of magmatic zircons (Ce/Ce^* 32–49) [42]. Weak positive Eu anomalies (Eu/Eu^* 0.96–1.27) are observed in these zircons contrasting to the common negative Eu anomalies (Eu/Eu^* <1) in the magmatic zircons. The LREE are relatively enriched with $(Sm/La)_N$7.62–29.46 (except two zircon grains with 79.36 and 48.67, respectively). These $(Sm/La)_N$ values are evidently lower than that of magmatic zircon (22–110). In summary, the REE compositions of zircons in the altered alkaline syenites bearing MW-type tetrad effect as demonstrated by the smoother patterns without pronounced Ce anomalies and weaker HREE enrichment and M-type-like tetrad effect as well. These patterns are obviously different from those of magmatic zircons bearing evident positive Ce anomolies and steep left declined (HREE strongly enriched) REE patterns (Figure 6(a)). These features are clearly shown in the plot of $(Sm/La)_N$–La and Ce/Ce^*-$(Sm/La)_N$ (Figure 7). The altered alkaline syenites bearing MW-type tetrad effect are plotted in the transition area between magmatic and hydrothermal zircons and close to the hydrothermal zircon indicating the characters of hydrothermal reworked zircons.

2.3 The generation of MW-type of tetrad effect

(1) A multi-episodic superimposed magma-fluid system.

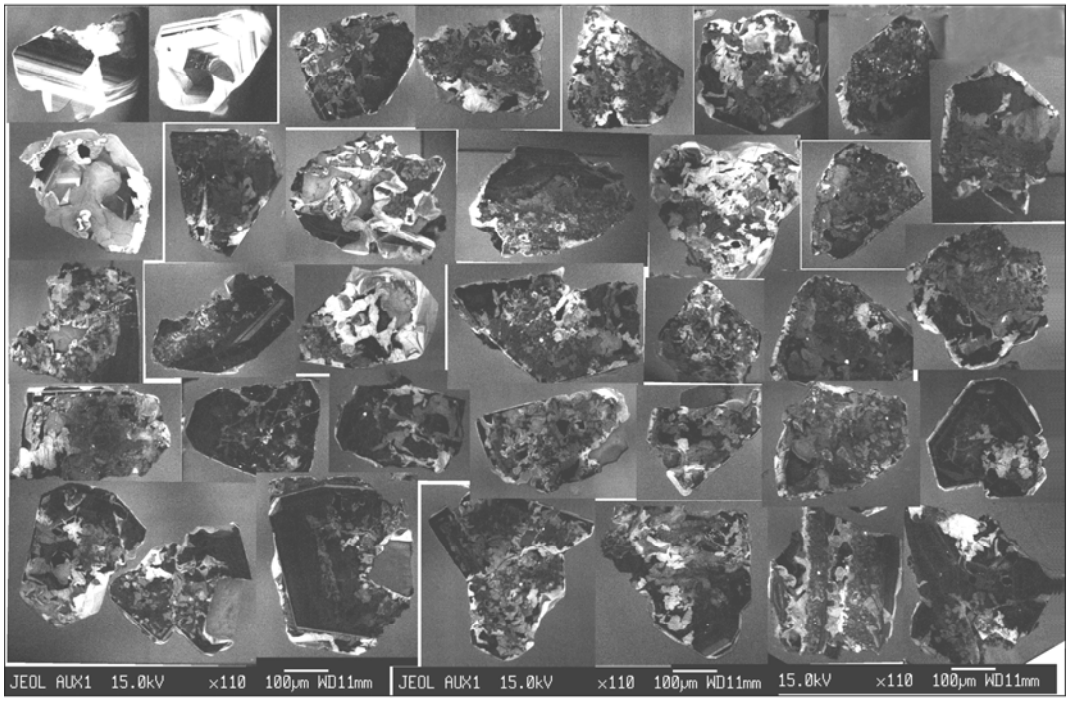

Figure 5 Cathodoluminescence images of zircons from altered alkaline syenite.

Table 5 REE contents of zircons from altered alkaline syenite (μg/g)

Analyses point	APR21 Q43	APR21 Q44	APR21 Q45	APR21 Q46	APR21 Q47	APR21 Q48	APR21 Q49	APR21 Q50	APR21 Q52	APR21 Q53	APR21 Q54	APR21 Q55	APR21 Q56	APR21 Q57	APR21 Q58
La^{139}	13	44.4	2.206	4.45	12.97	21.73	16.43	36.51	1.819	1.019	7.8	2.63	0.0172	11.78	99.65
Ce^{140}	345.8	488.54	410.03	103.65	192.3	270.85	267.74	473.59	37.33	346.45	188.34	106.84	16.89	246.9	1619.6
Pr^{141}	36.55	87.72	10.86	14.44	22.9	46.86	32.2	76.12	3.64	6.44	23.74	9.33	0.108	35.77	256.09
Nd^{143}	247.52	558.69	98.95	101.14	156.36	296.84	212.44	482.43	26.58	57.52	166.01	69.99	1.073	245.27	1702.7
Sm^{147}	104.28	212.2	67.58	35.58	100.77	111.19	102.59	169.38	14.93	18.65	75.04	48.79	0.862	102.42	733.96
Eu^{151}	49.24	94.22	36.09	14.21	56.7	46.58	49.62	72.44	5.5	6.69	33.78	22.74	0.526	43.6	339.6
Gd^{157}	137.75	235.2	125.75	43.91	183.82	123.39	150.08	187.22	20.41	18.44	104.8	78.18	2.5	130.46	919.71
Tb^{159}	26.23	45.5	23.75	8.26	34.28	22.5	31.47	33.79	4.71	2.443	21.77	15.94	0.754	26.39	176.91
Dy^{163}	180.82	321.2	157.81	64.74	236.15	147.48	236.77	224.58	42.68	15.15	163.38	116.44	7.48	200.76	1196.92
Ho^{165}	44.27	76.46	36.52	18.77	60.08	34.91	64.43	54.21	14.39	3.32	44.79	29.37	2.96	54.84	282.16
Er^{166}	149.43	248.54	102.64	74.1	214.79	110.85	247.91	175.53	64.42	10.22	168.31	99.73	14.61	210.27	893.58
Tm^{169}	32.02	51.9	16.67	17.13	45.07	21.29	55.29	32.74	15.75	1.817	35.65	19.55	4.01	46.24	161.75
Yb^{173}	320.99	503.11	124.5	184.28	449.67	193.08	556.28	292.28	170.76	17.88	340.6	177.11	49.08	461.05	1346.55
Lu^{175}	46.07	73.03	18.43	37.2	87.65	33.55	102.44	51.88	35.46	3.62	61.09	30.7	11.74	82.84	203.85
Ti^{49}	435.45	26.2	36.27	9.68	5.78	14.33	18.93	27.19	24.7	434.68	3.84	5.43	18.14	3.43	22.74
Y^{89}	1543.98	2597.22	1208.24	712.81	2092.57	1258.52	2317.72	1979.23	494.64	139.66	1604.46	964.81	146.32	1986.64	10105.81
Zr^{90}	361276	364210	443784	428803	405834	419780	401409	411299	436557	442538	443377	424744	423398	377264	443150
Th^{232}	931.95	1349.51	941.28	224.62	1590.61	553.21	4313.27	1014.55	187.58	1070.77	758.99	321.61	38.46	754.93	2458.69
U^{238}	3820.95	2277.66	1076.61	1226.52	2290.28	986.32	3421.69	2088.47	688.86	772.88	2190.17	813.81	222.96	2181.41	4869.88

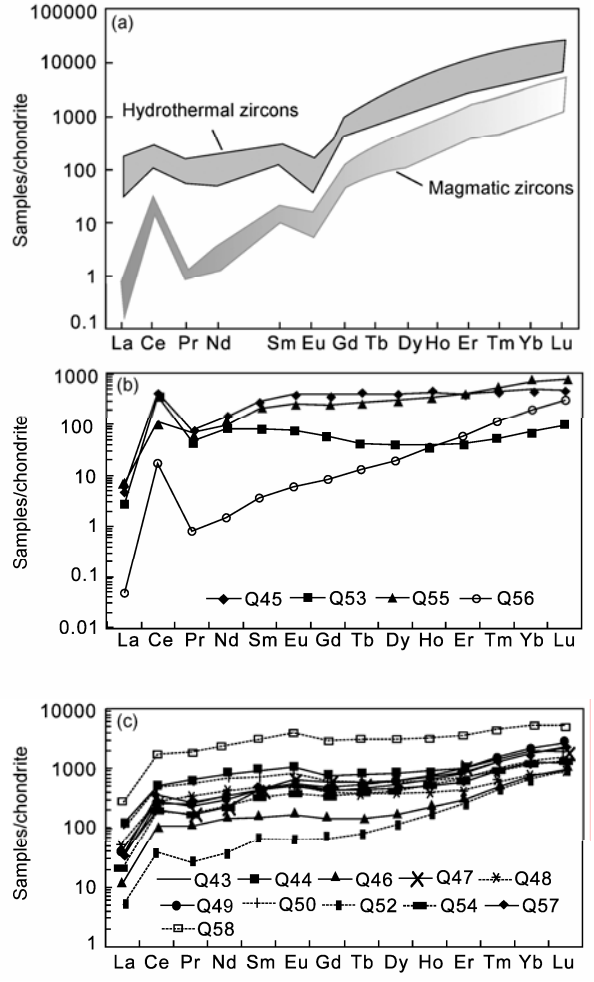

Figure 6 Chondrite-normalized REE patterns of zircons from K-feldspar altered and silicificated alkaline synites.

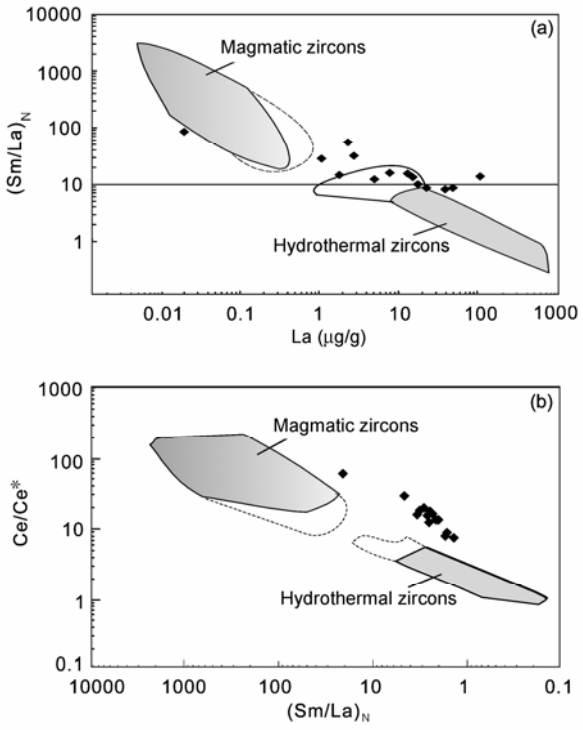

Figure 7 Discrimination plots for magmatic and hydrothermal zircon (after Hoskin [42]).

The coexistence of magmatic and hydrothermal apatite and zircon in altered alkaline syenite bearing MW-type tetrad effect reveals that the MW-type tetrad effect was initiated in an opened and superimposed hydrothermal system. The REE patterns of apatites suggest the altered alkaline syenites bearing the MW-type tetrad effect were superimposition of two processes: the strong fractional crystallization of alkaline

magma and the strong LREE (La-Nd) leaching by two different kinds of hydrothermal fluids as evidenced by the REE patterns of the two subgroups of apatite.

Since the 1990s different isotopic dating methods were carried out for the Shuiquangou alkaline syenites mainly because of the related Au mineralization. The reported isotopic ages vary in a wide range of 300–1718 Ma (Table 6). Hence, more precise isotopic datings are needed to verify the time frame for the syenits and the hydrothermal fluids related Au mineralization. Miao et al. [48] reported the SHRIMP zircon U-Pb age of 390±6 Ma which was believed to be the crystallization age of the Shuiquangou alkaline syenites. Systematic SHRIMP zircon U-Pb dating of the igneous rocks in the area showed that there are three epochs of magmatism [48,50,51]: 390± Ma (middle Devonian) for Shuiquangou alkaline syenites; 235± Ma (middle Triassic) for Honghualiang and Guzuizi biotite granites and 130± Ma (early Cretaceous) for Shangshuiquan alkaline granite, Zhuanzhilian diorite and Zhangjiakou group volcanic rocks.

Table 6 shows a wide range of mineralization age spectrum (350–153 Ma) [47–58]. Li et al. [49] reported conventional isotopic dilution U-Pb dating on individual zircon grains from auriferous quartz vein which gave a result of 350.9±0.9 Ma and was interpreted as the age of Au mineralization.] Our analysis of 61 single zircons from altered alkaline syenites with MW-type tetrad effect dated using LA-ICPMS method display a wide range of ages (394–189 Ma, Figure 8). Among them 19 zircon grains plotted on the concordant line giving a weighted average $^{206}Pb/^{238}U$ age of 389.9±1.7 Ma representing the age of syenite crystallization; while 9 zircon grains give nearly concordant weighted average $^{206}Pb/^{238}U$ age of 357.6±3.5 Ma consisting with the isotopic dilution U-Pb age of zircon reported by Li et al. [49] and may represent an important mineralization epoch.

The $^{40}Ar/^{39}Ar$ dating of K-feldspar, sericite and quartz have yielded a age spectrum ranging from 153–289 Ma [47,50,53–58]. These data suggest that the hydrothermal fluid activity or Au mineralization lasted from the late Paleozoic to late Mesozoic, i.e. about 250 Ma. The $^{40}Ar/^{39}Ar$ age spectrum might be related with magmatic activities of

Table 6 Isotopic ages of alkaline syenites, Shuiquangou and adjacent igneous rocks and gold deposits

Location	Sample	Method	Age (Ma)	Reference
Shuiquangou alkaline syenite				
Dongping	alkaline syenite, zircon	SHRIMP U-Pb	390±6	[48]
Hougou	syenite, zircon	SHRIMP U-Pb	386±7	[48]
Xiasandaohe	quartz syenite, zircon	Isotopic dilution U-Pb	410.2±1.1	[49]
Xialiangjianfang	amphibole syenite, amphibole	$^{40}Ar/^{39}Ar$	327.4±9	[52]
Shuiquangou	syenite, K-feldspar	$^{40}Ar/^{39}Ar$	305.9±0.5	[56]
Hougou	syenite, K-feldspa	$^{40}Ar/^{39}Ar$	304.5±0.5	[56]
Huangtuliang	syenite, K-feldspar	$^{40}Ar/^{39}Ar$	304.9±0.5	[56]
Dongping	syenite, zircon	U-Pb	1718±65 (upper intercepted point) 454±40 (lower intercepted point)	[59]
Dongping	potassic and silicificated syenite, zircon	LA-ICPMS,U-Pb	389.8±1.2	this study
Granites and volcanic rocks in adjacent area of Shuiquangou				
Guzuizi	porphyritic granite, zircon	SHRIMP U-Pb	236±2	[48]
Honghualiang	biotite granite, zircon	SHRIMP U-Pb	235±2	[50]
Zhuanzhilian	Diorite, zircon	SHRIMP U-Pb	139.5±0.9	[50]
Shangshuiquan	alkaline granite, zircon	SHRIMP U-Pb	142.5±1.3	[48]
Zhangjiakou formation	rhyolite, zircon	LA-ICPMS	126±1	[51]
Houcheng formation	dacite, zircon	LA-ICPMS	130±1	[51]
Gold deposit				
Dongping	Au lode, zircon	U-Pb	350.9±0.9	[49]
Dongping	altered wall rock of au lode, zircon	LA-ICPMS U-Pb	357.6±3.5	this study
Dongping	Au lode, K-feldspar	$^{40}Ar/^{39}Ar$	177.4±5	[52]
Dongping	Au lode, K-feldspar	$^{40}Ar/^{39}Ar$	156.7±0.88	[53]
Dongping	altered wall rock of AU lode, K-feldspar	$^{40}Ar/^{39}Ar$	289.1±0.3	[56]
Hougou	Au lode, Quartz	$^{40}Ar/^{39}Ar$	177.6±1.9	[54]
Hougou	altered wall rock of Au lode, K-feldspar	$^{40}Ar/^{39}Ar$	172.9±5	[55]
Hougou	altered wall rock of Au lode, K-feldspar	$^{40}Ar/^{39}Ar$	288.1±0.4	[56]
Dongping	altered wall rock of Au lode, Sericite	$^{40}Ar/^{39}Ar$	186.8±0.3	[54]
Hougou	altered wall rock of Au lode, Sericite	$^{40}Ar/^{39}Ar$	187.9±0.4	[56]
Huangtuliang	altered wall rock of Au lode, Sericite	$^{40}Ar/^{39}Ar$	187.4±0.3	[56]
Hougou	Au lode, K-feldspar	Laser $^{40}Ar/^{39}Ar$	202.6±1.0 –176.7±1.6	[57]
Zhongshangou	altered wall rock of Au lode, K-feldspar	$^{40}Ar/^{39}Ar$	241±1 (max) 180 (min)	[58]
No.70 Au lode, Dongping	altered wall rock of Au lode, Muscovite	$^{40}Ar/^{39}Ar$	153±3 (excess argon)	[58]
No.70 Au lode, Dongping	altered wall rock of Au lode, Muscovite	$^{40}Ar/^{39}Ar$	153±2 (excess argon)	[58]

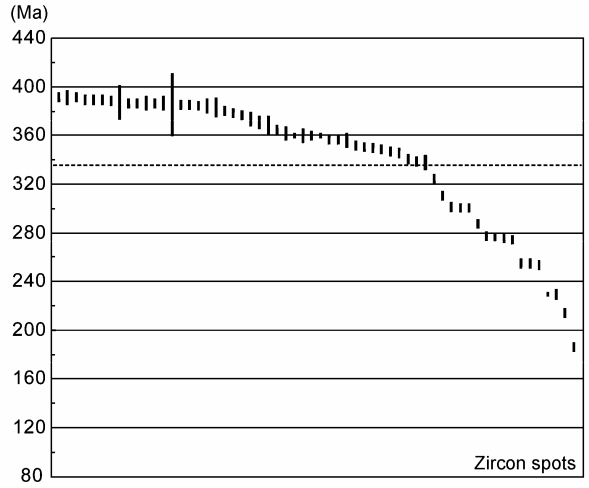

Figure 8 U-Pb age spectrum of zircons from Shuiquangou altered alkaline syenite.

390, 235 and 130 Ma in the Shuiquangou area. The LA-ICPMS dating spectrum of hydrothermal zircons reflects these geothermal events and indicates that the long and multi-episodic interaction between syenites and fluids which result in redistribution of REE between melt (rock) and fluids and, thus, should be responsible for the forming of MW-type tetrad effect.

(2) Characteristics of the melt and fluid systems. As discussed above, the igneous rocks bearing REE tetrad effect are commonly high evolved and closely associated with W, Sn and rare-metal mineralization. The rocks are commonly alkali-rich and underwent intensive potash and/or sodic alteration and silicification. The complexation of alkaline metals and REE along with the halogens (F, Cl) and CO_2, P released from the highly evolved magma might play an important role in the generation of REE tetrad effect. According to the contents of mafic minerals the Shuiquangou alkaline syenites can be divided into augite amphibole alkali feldspar syenite, amphibole alkali feldspar syenite and minor quartz monzonite, they are distributed WE-trending and no clear boundaries between them. As the rock type changes from amphibole syenite to quartz syenite eastwards the contents of major rock-forming elements change gradually, for example, Si and felsic element contents increase and mafic element contents decrease which shows the proceeding of fractional crystallization. In addition, the REE contents decrease while the chondrite-normalized REE patterns of these rocks keep nearly same forms indicating no obvious REE fractionation except for the quartz monzonite [47]. Different types of inclusions including melt, fluid and fluid-vapor inclusions in quartz of the altered alkaline syenite were observed. The melt inclusions consist of glass+vapor, glass+crystals and glass+vapor+crystals with homogeneous temperature of 900–925°C [55,59,60]. There are two-phase fluid inclusions (fluids+vapor H_2O), CO_2-rich two phase inclusions (fluids+vapor CO_2) and CO_2-bearing three-phase inclusions (liquid and vapor CO_2, liquid H_2O) in auriferous quartz veins. Moderate-low salinity (5%–13% NaCl) [58], homogeneous temperature 140–390°C of inclusions in quartz and main mineralization temperature (372–306°C)were reported. The contents of F, Cl and CO_2 in inclusions of the hydrothermal quartz are 0.05×10^{-6}–10.7×10^{-6}, 0.22×10^{-6}–40.7×10^{-6} and 4.5×10^{-6}–129×10^{-6}, respectively, and the Cl/F rages from 1.24 to 54 (very few up to 202) [61–64]. Hydrogen and oxygen isotopic compositions of the fluids show the transition between magmatic and meteoric waters and closing to the magmatic water implying their mixed resources.

In summary, the Shuiquangou altered alkaline syenites bearing MW-type tetrad effect must have been the results of two stage modifications: (1) interaction of magma with co-existing fluids, and (2) metasomatism of syenites by NaCl-CO_2-H_2O type fluids with high temperature and moderate-low salinity, i.e. hydrothermal solutions which are rich in Cl, CO_2 and low in SO_4^{-2}[65].

(3) Alteration. The alkaline syenites bearing MW-type tetrad effect can be divided into two kinds based on the alteration intensity: one is potassic alteration in the form of K-feldspar showing the K-feldspar developed at the upper and lower walls of the Au-bearing veins such as the No. I Au lode and No. 2, No. 22 Au lode; the second is composite alteration of silicification, K-feldsparization and pyritization developed along mass fine cracks and cleavages such as the No. 70 Au lode. The alteration consisted mainly of K-feldspar distributed symmetricly along the two sides of the Au lode (Figure 9). In addition, the sericitization and carbonatization are also common in the ores.

Barth method is used to describe the mobilities of major elements during alteration process from a section in No.70 Au lode which shows that the relative contents of SiO_2, Al_2O_3 and K_2O increased 4%, 23% and 13% respectively, on the contrary, the relative contents of Fe_2O_3, FeO and CaO decreased 71%, 19% and 60%, respectively, during the potassic

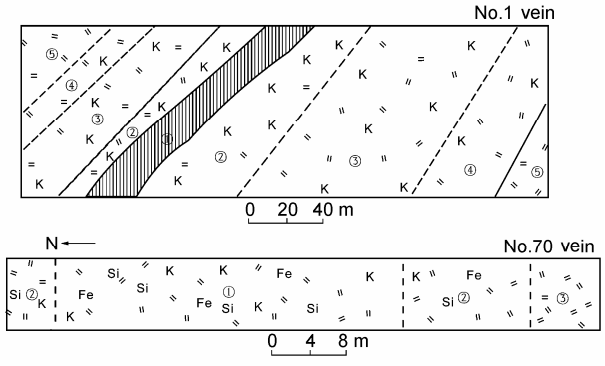

Figure 9 Sketch map of alteration in the Shuiquangou alkaline syenites. No. 1 Au lode: ① Au-bearing lode; ② strong potassic alteration; ③ moderate-strong potassic alteration; ④ weak potassic alteration; ⑤ alkaline syenite. No. 70 Au lode: ① strong potassic and silicification alteration; ② weak potassic and silicification alteration; ③ alkaline syenite.

alteration. The relative contents of SiO_2, increased up to 24% during potassic and silicification alterations and the relative contents increased 23%, 20%, 86%, 68%, 22% for K_2O, Fe_2O_3, FeO, CaO and K_2O, respectively, for intensive silicification alteration. Similar features are shown in the No.1 Au lode.

The REEs are usually stable during various magmatic processes. Obvious mobilities of REEs were observed in hydrothermal alteration and their mobilities increase with the increase of fluids/melts or fluids/rock ratios [29,66–70]. From (augite) amphibole alkaline syenite to alkaline syenite, the REE contents exhibit systematic decrease with not evident changes of LREE/HREE and Eu anomolies reflecting the evolution of alkaline magma. More importantly, drastically decrease of $\sum$REE particular the LREE contents are observed in the altered alkaline syenite bearing MW-type tetrad effect, the lowest $\sum$REE contents exist in the silicified Au ores with $\sum$REE<10 μg/g particular the LREE decreased evidently with $(La/Yb)_N$<10. The changes of Eu anomaly are not clear. The average ratios of Y/Ho range from 25.6 to 31.7 with average 29.4 nearly the chondrite value 28 in the unaltered alkaline syenite, the same features exist in strong silicified alkaline syenites showing Y/Ho range 21.8–25.6 and average 23.7. In contrast, the altered alkaline syenites bearing MW-type tetrad effect have significantly higher Y/Ho ratios, ranging from 28.3 to 39.0 with a mean value of 32.8. These characters reveal that the non-CHARAC trace element behaviour (non-chondritic Y/Ho ratio) is the features of the highly evolved magma system rich in volatiles H_2O, Li, B, F, P and/or Cl. Hence, the system with MW-type tetrad effect should be volatile-rich and strong compolexing. This consideration is supported by the facts mentioned above that the complexation with fluorine generates Y/Ho>28 while the complexation with bicarbonate is assumed to generate value s<28 [20].

The variation of REE composition of magmatic and hydrothermal apatites bearing M- and MW-type tetrad effects show a "miniature" of the MW-type forming processes during potassic and silicification alterations. The variation suggests that the processes from forming LREE-rich alkaline syenite to the HREE-rich altered alkaline syenite can be divided into two stages: the LREEs were strongly leached in the first stage resulting in the LREE contents decrease to about 1/3, $(La/Yb)_N$ to 1/4–1/6 that of the original and the HREE contents doubled. In the second stage the HREE contents increase and LREE contents decrease with the $(La/Yb)_N$ decrease to 2–3 orders of magnitude. In contrasting, the $\sum$REE contents, the LREE in particular, increase evidently from the magmatic to hydrothermal altered zircons. The $(La/Yb)_N$ ratios increase from 0.0002 to 0.084 (increase about more than 400 times). The LREE leached from the apatites might have been incorporated into the hydrothermal zircons which resulted in the typical M-type tetrad effect different from those of the magmatic zircons (Figure 6).

Another pronounced character of the hydrothermal altered zircons in the alkaline syenite bearing MW-type is that they are rich in U and Th. The ^{238}U contents range from 537.5 μg/g to 26844 μg/g, mostly n×1000 μg/g and ^{232}Th contents range from132.6 μg/g to 12244 μg/g, mostly about 1000 μg/g, only 4 zircon grains have rather low contents of U and Th (93.83–459 μg/g and 13.05–71.55 μg/g, respectively). The U and Th contents of hydrothermal zircons are obviously higher than those of zircons in unaltered alkaline syenite with ^{238}U contents 43–564 μg/g and ^{232}Th contents 6–308 μg/g. These hydrothermal zircons have high and more variable Th/U ratios (0.08–2.07, averaging 0.45) which are distinguishable from that of magmatic zircons with lower and less variable Th/U ratios (0.08–0.51, averaging 0.22) within the unaltered alkaline syenite [48]. Only 3 out of the 61 zircon grains analysed show ratios lower than 0.10. In general, the lower Th/U ratios (<0.10) of metamorphic or hydrothermal zircons are different from that of magmatic zircons [71–74] because that the bigger Th ionic radius (Th^{+4} 0.105 nm) than that of U (Th^{+4} 0.100 nm) may cause unstable of zircon crystal lattice and easily be brought out of zircon resulting in the decreasing of Th/U. The unusually Th/U ratios suggest that the hydrothermal fluids forming the MW-type tetrad effect should be rich in chloride and carbon which is supported by the inclusion compositions. The solubility of Th is very low in this kind of fluids and the fluid-zircon interaction results in high Th/U ratios of zircons [75].

The radiogenic Pb in zircons may be lost during hydrothermal alteration resulting in lower U-Pb ages [75], a complex unconcordant age spectrum, and more variable zircon U-Pb ages (394–189 Ma) in the altered alkaline syenite (Figure 8).

In recent years, experimental researches on REE behaviour in hydrothermal alteration systems gave the evidence for the forming of tetrad effect. Using biotite granite without tetrad effect as the starting materials react with NaCl solution under 150 MPa and 850°C, the quenched glass of experiment products exhibit M-type tetrad effect [21]. New results on neodymium (III) aqua and chloroaqua complex in aqueous solutions to 500°C and 520 MPa performed by Mayanovic et al. [30] provide the data of structure and stability of aqueous REEs in hydrothermal fluids and reveal that the mobility and fractionation of REEs are controlled by the availability of and the degree of complexation with ligands such as Cl^-, F^-, PO_3^-, CO_3^{2-} and SO_4^{2-}, the pH of the fluids and redox conditions. The reduction of the first-shell water molecules with temperature for Nd^{+3} is intermediate between the rate for Gd^{+3}, $Eu^{+3}$and Yb^{+3} aqua ions indicating an intermediate stability of the Nd^{+3}aqua ion consistent with the tetrad effect. According to these data we presume that the forming of MW-type tetrad effect are controlled by the multi-episodic alterations of high temperature hydrothermal fluids rich in Cl, CO_2, Si, K and Al. This system is obviously different from that of M-type tetrad effect forming by interaction of F-rich fluids with melts and that of W-type tetrad effect forming from low temperature fluids.

3 Conclusions

(1) A new type of REE tetrad effect, a composite M- with W-type, was recognized in the K-feldsparthized and silicificated alkaline syenite complex, Dongping Shuiquangou, Hebei Province, it possesses the characteristics of both M-type and W-type tetrad effects;

(2) REE compositions of apatites and zircons in altered alkaline syenite bearing MW-type tetrad effect reveal that the hydrothermal alterations in at least two-stage hydrothermal activities were superimposed on the fractional crystallization of magma which lead to the generation of the composite M- with W-type REE tetrad effect;

(3) Coexisting of melts with fluids and the superimposed alteration of volatiles $(Cl,CO_2)^-$ and Si, Al-enriched high temperature, moderate-low salinity hydrothermal fluids might be main controlling factors for the formation of MW-type tetrad effect. In addition, the peculiar MW-type of tetrad effect provides available information for the reworked-type of Au mineralization processes and can be as a potential indicator for Au mineralization;

(4) The U-Pb and $^{40}Ar/^{39}Ar$ isotopic ages of the zircons and hydrothermal altered minerals suggest that the alteration and the forming of MW-type tetrad effect might be a prolonged process and multi-episodic reworking and record the Au mineralization in alkaline complex magmatic system.

Importantly, regarding the complexity of the hydrothermal alteration, in the future studies of the forming of MW-type tetrad effect, more detailed investigation on isotopic dating and oxygen isotopic and trace element composition of altered minerals and individual inclusions should be carried out.

The authors thank two anonymous reviewers for their thoughtful and constructive comments. Also they thank Dr. Liu Xiaoming, Tu Xianglin and Hu Guangqian for their help in the isotopic dating of zircons, and analyses of REE compositions of apatites, zircons and alkaline syenites. This work was supported by the National Natural Science Foundation of China (40773018) and the National Basic Research Program of China (2006CB403504). This is contribution No. IS-1124 from GIGCAS.

1 Henderson P. General geochemical properties and abundances of the rare earth elements. In: Henderson P, ed. Rare Earth Element Geochemistry. Amsterdam: Elesevier, 1984. 8–9
2 Masuda A. Regularities in variation of relative abundances of lanthanide elements and an attempt to analyse separation-index patterns of some minerals. J Earth Sci Nagoya Univ, 1962, 10: 173–187
3 Coryell C G, Chase J W, Winchester J W. A procedure for geochemical intepratation of terristerial rare-earth abundance patterns. J Geophys Res, 1963, 68: 559–566
4 Masuda A, Ikeuchi Y. Lanthanide tetrad effect observed in marine environment. Geochem J, 1979, 13: 19–22
5 Hidaka H, Holliger P, Shimizu H, et al. Lanthanide tetrad effect observed in the Oklo and ordinary uraninites and its application for their forming processes. Geochem J, 1992, 26: 337–346
6 Akagi T, Shabani M B, Masuda A. Lanthanide tetrad effect in kimuraite $[CaY_2(CO3)_4{\cdot}6H_2O]$: Implication for a new geochemical index. Geochim Cosmochim Acta, 1993, 57: 2899–2905
7 Takahashi Y,Yoshida H, Sato N, et al. W-and M-type tetrad effects in REE patterns for water-rock systems in the Tono uranium deposit, central Japan. Chem Geol, 2002, 184: 311–335
8 Zhao Z H. Preliminary report on the REE tetrad effect in granites (in Chinese). Geol Geochem, 1988,1: 71–72
9 Zhao Z H. REE tetrad effect-an important indicator for water/melts (rock) interaction (in Chinese). In: Proceedings of the 3rd Congress on Mineralogy, Petrology and Geochemistry Symposium of China. Chongqing: Chongqing Branch of Science and Technology Press of China, 1988. 47–49
10 Zhao Z H, Masuda A. REE evidence for warter-rock interaction in tin/tungsten granites. In: The Fifth International Symposium on Tin/Tungsten Granites in Southeast Asia and the Western Pacific, Matsue, Japan (Extended abstract), 1988. 257–258
11 Masuda A, Kawakami O, Dohmoto Y, et al. Lanthanide tetrad effects in nature: two mutually opposite types, W and M. Geochem J, 1987, 21: 119–124
12 Fideslis I, Siekierski S. The regularities in stability constraints of some rare earth complexes. J Inorg Nucl Chem, 1966, 28: 185–188
13 Peppard D F, Mason G W, Lewey S. A tetrad effect in the liquid-liquid extraction ordering of lanthanides (III). J Inorg Nucl Chem, 1969, 31: 2271–2272
14 Zhao Z H, Masuda A, Shabani M B. Tetrad effect in rare metal granites (in Chinese). Geochimica, 1992, 3: 221– 233
15 Zhao Z H, Masuda A, Shabani M B. REE tetrad effects in rare metal granite. Chin J Geochem, 1993, 12: 206–219
16 Jolliff B L, Papike J J, Shearer C K. Inter- and intro-crystal REE variations in apatite from the Bob Ingersoll Pegmatite, Black Hills, South Dakota. Geochim Cosmochim Acta, 1989, 53: 429–441
17 Yurimoto H, Duke E F, Opapike J J, et al. Are discontinuous chondrite-normalized REE patterns in pegmatic granite systems the results of monazite fractionation? Geochim Cosmochim Acta, 1990, 54: 2141–2145
18 McLennan S M. Rare earth element geochemistry and the "tetrad" effect. Geochim Cosmochim Acta, 1994, 58: 2025–2033
19 Bau M. Controls on the fractionation of isovalent trace elements in magmatic and aqueous systems: Evidence from Y/Ho, Zr/Hf and lanthanide tetrad effect. Contrib Mineral Petrol, 1996, 123: 323–333
20 Irber W. The lanthanide tetrad effect and its correlation with K/Rb, Eu/Eu*, Sr/Eu, Y/Ho and Zr/Hf of evolving peraluminous granite suits. Geochim Cosmochim Acta, 1999, 63: 489–508
21 Zhao Z H, Xiong X L, Han X D. Discussion on the forming of REE tetrad effect in granites (in Chinese). Sci China Ser D, 1999, 29: 331–338
22 Zhao Z H, Xiong X L, Han X D, et al. Controls on the REE tetrad effect in granites: Evidence from the Qianlishan and Baerzhe granites, China. Geochim J, 2002, 36: 527–543
23 Moneck T, Kemfe U, Monecke J, et al. tetrad effect in rare earth element distribution patterns: A method of quantification with application to rock and mineral samples from granitic-related rare metal deposits. Geochim Cosmochim Acta, 2002, 66: 1185–1196
24 Liu C Q, Zhang H. The lanthanide tetrad effect in apatite from the Altay No.3 pegmatite, Xinjiang, China: An intrinsic feature of the pegmatite magma. Chem Geol, 2005, 214: 61–77
25 Ji J F. M-type REE tetrad effect of low temperature stibnite and its geochemical significances in west Hunan (in Chinese). Bull Mineral Petrol Geochem, 1993, 70
26 Peng J T, Hu RZ, Zhao J H, et al. REE geochemistry of scheelites in W-Sb-Au deposits in west Hunan (in Chinese). Geochimica, 2005, 34: 115–122
27 Hong W X, He S Y, Huang S H, et al. W-type of REE tetrad effect of monazite and its geological significance (in Chinese). Prog Nat Sci, 1999, 9(Supp): 1287–1290
28 Liu C Q, Masuda A, Okada A, et al. Ageochemical study of loess and desert sand in northern China: Implication for continental crust weathering and composition. Chem Geol, 1993,106: 359–374
29 Veksler I V, Dorfman A M, Kamenetsky M, et al. Partitioning of lanthanides and Y between immiscible silicate and fluoride melts, fluorite and cryolite and the origin of the lanthanide tetrad effect in igneous rocks. Geochim Cosmoch Acta, 2005, 69: 2847–2860
30 Mayanovic R A, Anderson A J, Bassett W A, et al. The structure and stability of aqueous rare-earth elements in hydrothermal fluids: New

results on neodymium (III) aqua and chloroaqua complex in aqueous solutions to 500 and 520 MPa. Chem Geol, 2009, 259: 30–38
31 Zhao Z H, Bao Z W, Lee Seung-Gu, et al. A composite M- With W-type of REE tetrad effect in a north China alkaline complex. Geochim Cosmochim Acta, 2008, 72(Supp): 11095
32 Liu Y, Liu H C, Li X H. Simultaneous and precise determination of 40 trace elements in rock samples using ICP-MS. Geochimica, 1996, 25: 552–558
33 Yuan H L, Gao S, Liu X M, et al. Accurate U-Pb age and trace element determinations of zircons by laser ablation-inductively coupled plusma-mass spectrometry. Geos Geoanal Res, 2004, 28: 1511–1520
34 Guo C J. Mineralogical Chemistry of Rare Elements (in Chinese). Beijing: Science Press, 1965. 227–228
35 Wang Z G, Yu X Y, Zhao Z H. Rare Element Geochemistry (in Chinese). Beijing: Science Press, 1989. 58–62
36 Watson E B, Green T H. Apatite/liquid partition coefficients for the rare earth elements and strontium. Earth Planet Sci Lett, 1981, 56: 408–421
37 Fujimaki H. Partition coefficients of Hf, Zr and REE between zircon, apatite and liquid. Contrib Mineral Petrol, 1986, 94: 42–45
38 Ayers J C, Watson E B. Apatite/fluid partitioning of rare-earth elements and strontium: experimental results at 1.0 GPa and 1000°C and applications to models of fluid-rock interaction. Chem Geol, 1993, 110: 299–314
39 Rubin J N, Henry C D, Price J G. Hydrothermal zircons and zircon overgrowths, Sierra Blanca Peaks, Texas. Am Mineral, 1989, 74: 865–869
40 Kerrich R, King R. Hydrothermal zircon and baddeleyite in Val-Dor Archean mesothermal gold deposits: Characteristics, compositions and fluid-inclusion properties, with implications for timing of primary gold mineralization. Can J Earth Sci, 1993, 30: 2334–2352
41 Hoskin P W O, Schaltegger U. The composition of zircon and igneous and metamorphic petrogenesis. In: Hanchar J M, Hoskin P W O, eds. Zircon. Rev Mineral Geochem, 2003, 53: 27–62
42 Hoskin P W O. Trace-element composition of hydrothermal zircon and the alteration of hadean zircon from the Jack Hills, Australia. Geochim Cosmochim Acta, 2005, 69: 637–648
43 Fu B, Page F Z, Cavosie A J, et al. Ti-in-zircon thermometry: Applications and limitations. Contrib Mineral Petrol, 2008, 156: 197–215
44 Hoskin P W O. Minor and trace element analysis o f natural zircon ($ZrSiO_4$) by SIMS and laser ablation ICPMS: A consideration and comparison of two broadly competitive techniques. J Trace Microprobe Tech, 1998, 16: 301–326
45 Wu Y B, Zheng Y F. Constraints on the interpretation of Zircon U-Pb dating based on the investigation of the zircon mineralogy (in Chinese). Chin Sci Bull, 2004, 16: 1589–1603
46 Xie L, Wang R C, Wang D Z et al. Hydrothermal zircon—A unusual zircon (in Chinese). In: Chen J, ed. Prog Geol Geochemi. Nanjing: Nanjing University Press, 2006. 325–333
47 Song G R, Zhao Z H. Geology of Dongping Alkaline Complex-hosted Gold Deposit in Hebei Province (in Chinese). Beijing: Seismic Publishing House, 1996. 1–170
48 Miao L C, Qiu Y M, McNaughton N, et al. SHRIMP U-Pb zircon geochronology of granitoids from Dongping area, Hebei Province, China: Constraints on tectonic evolution and geodynamic setting for gold metallogeny. Ore Geol Rev, 2002, 19: 187–204
49 Li H M, Li H K, Lu S N, et al. Determination of age of gold mineralization of Donping gold deposits by U-Pb dating hydrothermal zircons from ore veins (in Chinese). Acta Geosci Sin, 1997, 18(Supp): 176–178
50 Jiang N, Liu Y S, Zhou W G, et al. Derivation of Mesozoic adakitic magmas from ancient lower crust in the North China craton. Geochim Cosmochim Acta, 2007, 71: 2591–2608
51 Yang J H, Wu F Y, Shao J A, et al. *In-situ* U-Pb dating and Hf isotopic analyses of zircons from volcanic rocks of Houcheng and Zhangjiakou formations in the Zhangxuan area (in Chinese). Earth Sci J Chin Univ Geosci, 2006, 31: 71–80
52 Lu D L, Luo X Q, Wang J J, et al. Geochronological study on the Dongping gold deposit (in Chinese). Mineral Deposits, 1993, 12: 182–188
53 Hu D X, Luo G L. $^{40}Ar/^{39}Ar$ age of Au-bearing quartz veins in the Zhangjiakou and Xuanhua area (in Chinese). Sci Geol, 1994, 29: 151–158
54 Wang R R. The characteristics and genesis of the felsic alkali complex, Jinjiazhuang, Hebei (in Chinese). J Guilin Coll Geol, 1992, 12: 12–20
55 Jiang S H, Nie F J. $^{40}Ar/^{39}Ar$geochronology of the Shuiquangou alkaline complex and related gold deposit, Northwest Hebei, China (in Chinese). Geol Rev, 2000, 46: 621–627
56 Xu X W, Cai X P, Liu Y L, et al. Laser probe $^{40}Ar/^{39}Ar$ages of metasomatic K-feldspar from the Hougou gold deposit, northwest Hebei Province. Sci China Ser D-Earth Sci, 2002, 45: 559–564
57 Hart C J R, Goldfarb R J, Qiu Y M, et al. Gold deposits of the northern margin of the North China Craton: Multiple late Paleozoic-mesozoic mineralizing events. Miner Depos, 2002, 37: 326–351
58 Mo C H. The geochemistry and genesis of gold deposits in Zhangjiakou area (in Chinese). Dissertation for the Doctoral Degree. Guangzhou: Guangzhou Institute of Geochemistry, Chinese Academy of Sciences, 1996, 48
59 Xiang S Y, Ye J L, Liu J. The genesis of Hougou-Shuiquangou alkali-syenite rock mass and the relation between it and the mineralization of gold deposits (in Chinese). Geoscience, 1992, 6: 55–62
60 Song R X, et al. A research report on the characteristics, related Au mineralization and prospect of Shuiquangou-Dananshan monzonite complex in Zhangjiakou area (in Chinese). 1992
61 Wang Y, Jiang X M, Shang M Y, et al. The genesis and characteristics of gold deposits related with alkaline rocks in northwest Hebei (in Chinese). Geol Rev, 1994, 4: 368–376
62 Zhang Z C. Characteristics of H and O isotopes and fluid evolution in Dongping gold deposit (in Chinese). Gold Geol, 1996, 2: 36–41
63 Deng N D. Geology and prospect of gold deposits in Zhangjiakou area. A research report, 1988
64 Fan H R, Xie Y H, Zhai M G. Ore-forming fluids in the Dongping gold deposit, northwest Hebei Province. Sci China Ser D-Earth Sci, 2001, 44: 748–757
65 Alderton D H M, Pearce J A, Potts P J. Rare earth element mobility during granite alteration: Evidence from southwest England. Earth Planet Sci Lett, 1980, 49: 149–165
66 Humphris S E. The mobility of the rare earth element in crust. In: Henderson P, ed. Rare Earth Element Geochemistry. Amsterdam: Elsevier, 1984. 317–342
67 Grauch R I. Rare earth elements in metamorphic rocks. In: Lipin B R, McKay G A, eds. Geochemistry and rare earth elements. Rev Mineral, 1989, 21: 147–167
68 Bao Z W, Zhao Z H. Pare-earth element mobility during ore-forming process of Dongping gold deposit (in Chinese). Geochimica, 1998, 27: 81–90
69 Wood S A. The aqueous geochemistry of the rare-earth elements and yttrium 2. Theoretical predictions of speciation in hydrothermal solutions to 350°C at saturation water vapor pressure. Chem Geol, 1990, 88: 99–125
70 Schaltegger U, Fanning C M, Gunther D, et al. Growth, annealing and recrystallization of zircon and preservation of monazite in high-grade metamorphism conventional and *in-situ* U-Pb isotope, cathodoluminescence and microchemical evidence. Contrib Mineral Petrol, 1999, 134: 186–201
71 Hoskin P W O, Black J P. Metamorphic zircon formation by solid state recrystallization of protolith igneous zircon. J Metaph Geol, 2000, 18: 423–439
72 Rubattu D, Willianms I S, Buick I S. Zircon and monazite response to prograde metamorphism in the Reynolds Range, central Australia. Contrib Mineral Petrol, 2001,140: 458–468
73 Rubattu D. Zircon trace element geochemistry: Partitioning with garnet and the link between U-Pb ages and metamorphism. Chem Geol, 2002, 184: 123–138
74 Kebede T, Horie K, Hidaka H, et al. Zircon micro vein in peralkaline granitic gneiss, western Ethiopia: Origin, SHRIMP U-Pb geochronology and trace element investigations. Chem Geol, 2007, 242: 76–102
75 Whitehouse M J, Kamber B S. On the overabundance of light rare earth elements in terrestrial zircons and its implications for Earth's earliest magmatic differentiation. Earth Planet Sci Lett, 2002, 204: 333–346